1.5 Rare earth magnetism

The interactions discussed in the preceding section are the origin of the characteristic magnetic properties of the rare earth metals. The long-range and oscillatory indirect exchange gives rise to *incommensurable periodic structures*, the crystal fields and anisotropic two-ion coupling induce a *magnetic anisotropy* which may require fields up to hundreds of tesla to overcome, and the magnetoelastic interactions cause *magneto-strictive strains* which may approach one per cent. In the following, we shall give a brief description of some features of rare earth magnetism, as a prelude to a more detailed discussion of selected structures in the next chapter, and as a necessary basis for our later treatment of magnetic excitations. We have emphasized general principles, with appropriate illustrations, and have not attempted an exhaustive description of the magnetic properties of each element. This task has been accomplished by McEwen (1978), following earlier surveys by Rhyne (1972) and Coqblin (1977), and we shall refer to his comprehensive review article for further details, while quoting more recent investigations where appropriate.

Below the critical temperatures, listed in Table 1.6 on page 57, the rare earth metals form magnetically ordered phases. In the heavy elements, the maximum moment of $g\mu_B J$ per ion is approached in moderate fields at low temperatures. As is also apparent from Table 1.6, there is an additional contribution from the conduction electrons, which is almost 10% of the total moment in Gd, and appears to fall with S, as expected from (1.3.23). In their ordered phases, all the moments in a particular plane normal to the c-axis are aligned but, as illustrated in Fig. 1.19, their relative orientations may change from plane to plane. The magnetic structures of the heavy rare earths, which have been thoroughly reviewed by Koehler (1972) and Sinha (1978), derive basically from two different configurations of moments. In the *helix*, the expectation values

of the moments take the form:

$$\begin{aligned} \langle J_{i\xi} \rangle &= \langle J_{\perp} \rangle \cos(\mathbf{Q}\cdot\mathbf{R}_i + \varphi) \\ \langle J_{i\eta} \rangle &= \langle J_{\perp} \rangle \sin(\mathbf{Q}\cdot\mathbf{R}_i + \varphi) \\ \langle J_{i\zeta} \rangle &= 0, \end{aligned} \tag{1.5.1}$$

while the *longitudinal wave*, sometimes known in the heavy rare earths as the *c-axis modulated structure* or CAM, is described by

$$\langle J_{i\zeta} \rangle = \langle J_{\parallel} \rangle \cos(\mathbf{Q}\cdot\mathbf{R}_i + \varphi), \tag{1.5.2}$$

with the two other components being zero. The wave-vectors $\mathbf{Q}$ are along the c-axis, and the associated wavelength $2\pi/Q$ does not necessarily bear any simple relationship to the lattice spacing.

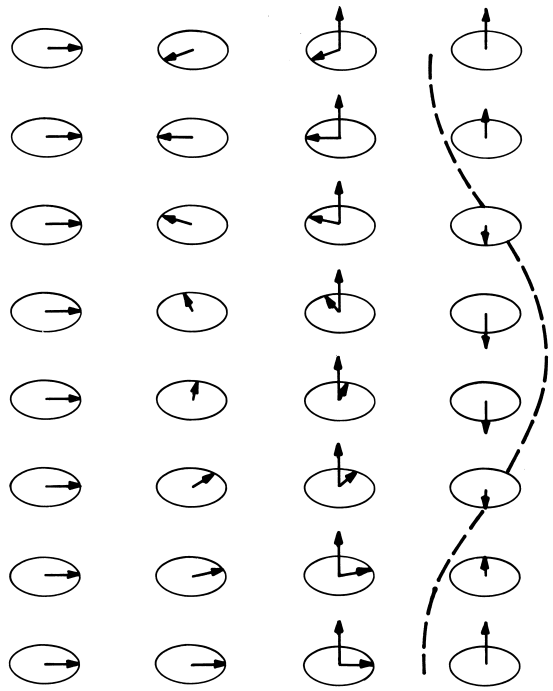

Fig. 1.19. Magnetic structures of the heavy rare earths. The moments in a particular hexagonal layer are parallel, and the relative alignments of different planes are illustrated. From left to right; the basal-plane ferromagnet, the helix, the cone, and the longitudinal-wave structure.

A helix is formed at the Néel temperature in Tb, Dy, and Ho, while the longitudinal-wave structure is preferred in Er and Tm. If the **Q**-vectors are zero, a *ferromagnetic structure* results, with the ordered moment along some specified direction. In Tb and Dy at low temperatures, the easy direction of magnetization lies in the plane, while in Gd, which has a very small magnetic anisotropy, it is along the c-axis just below the Curie temperature, but is tilted about 30° towards the b-axis at low temperatures. If a ferromagnetic component in the c-direction is added to the helix, the moments rotate on the surface of a cone with its axis in the c-direction. This *conical structure* is stable in both Ho and Er at the lowest temperatures, but the cone angle between the c-axis and the moments at 4 K is large (about 80°) in the former, and small (about 30°) in the latter. If the plane of the moments in the helix is rotated about an axis in the hexagonal plane, so that its normal makes a non-zero angle with **Q**, the structure becomes the *tilted helix*, which may be regarded as a combination of a helix and a longitudinal wave, with the same **Q**-vectors. This structure has not been definitively identified in the elements in zero field. The moments in the hexagonal plane of Er do order below 52 K, with the same period as the c-axis modulation, but they are most probably confined to the a–c plane, in an elliptically polarized *cycloidal structure* (Miwa and Yosida 1961; Nagamiya 1967) in the whole temperature interval between 52 K and the transition to the cone (Jensen 1976b). As the temperature is reduced, in the modulated c-axis phases, the moments on the individual sites approach their saturation values, resulting in a squaring of the longitudinal wave which manifests itself in higher odd harmonics. This phenomenon is observed in both Er and Tm and, in the latter, results in a low-temperature ferrimagnetic *square-wave structure* in which alternately four layers of moments point up and three layers point down.

The hexagonal anisotropy B_6^6 tends to distort the helical structure, by deflecting the moments towards the nearest easy axis. In a helix which is *incommensurable* with the lattice periodicity, this effect may be treated by perturbation theory, which predicts a change of the energy in second order. However, in Ho at low temperatures, B_6^6 is so large that the magnetic structure is forced to be *commensurable* with the lattice, so that **Q** has the magnitude $\pi/3c$, and the turn angle between the moments in successive planes averages 30°. It was verified experimentally by Koehler *et al.* (1966) that, under these circumstances, the large hexagonal anisotropy causes the helix to distort so that the moments in the plane bunch about the b-directions, as illustrated in Fig. 1.20. This *bunched helix* is described by

$$\begin{aligned} \langle J_{i\xi} \rangle &= \langle J_\perp \rangle (u \sin \mathbf{Q}\cdot\mathbf{R}_i - v \sin 5\mathbf{Q}\cdot\mathbf{R}_i) \\ \langle J_{i\eta} \rangle &= \langle J_\perp \rangle (u \cos \mathbf{Q}\cdot\mathbf{R}_i + v \cos 5\mathbf{Q}\cdot\mathbf{R}_i), \end{aligned} \qquad (1.5.3a)$$

where

$$u = \cos(\pi/12 - \phi) \quad ; \quad v = \sin(\pi/12 - \phi), \tag{1.5.3b}$$

and any moment deviates from the nearest b-axis by the *bunching angle* ϕ. At 4 K, ϕ in Ho is 5.8°, and it increases monotonically with temperature towards the value 15° which characterizes the uniform commensurable helix. An increase in temperature also causes an increase in $\mathbf{Q}$, but it was shown by Gibbs *et al.* (1985) that this change does not occur smoothly and continuously. Instead, the magnetic periodicity tends to lock in to values commensurable with the lattice, and they proposed that this is a manifestation of *spin-slip structures*, in which the moments are arranged in a pattern in which one of the planes in regularly spaced members of the bunched doublets of Fig. 1.20 is omitted, while the remaining plane of the pair orients its moments along the adjacent easy axis. We shall discuss such structures in more detail in the next chapter.

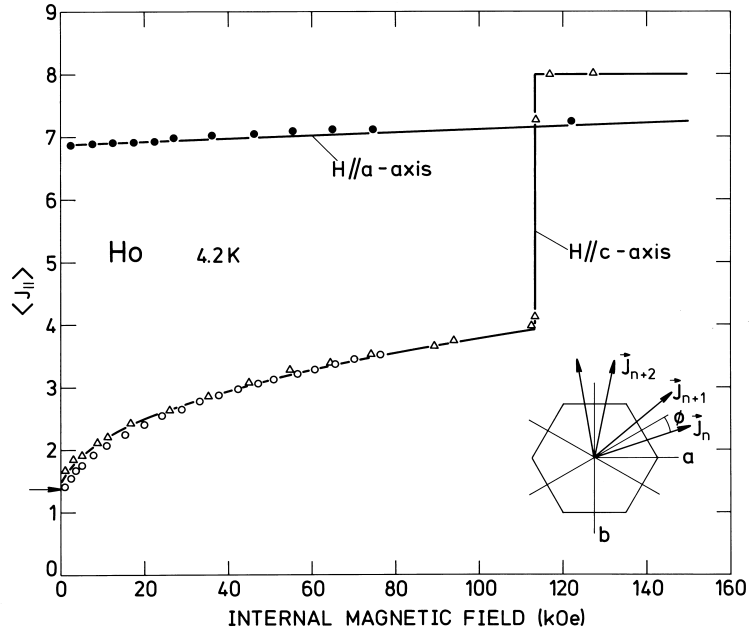

Fig. 1.20. The 4*f* contribution to the magnetization of Ho at 4 K, calculated by a self-consistent mean-field theory and compared with experimental values. The zero-field structure is a bunched cone, comprising the illustrated bunched helix in the plane, and a small moment in the *c*-direction. The value of the *c*-axis moment, deduced from neutron-diffraction measurements, is indicated by the arrow.

The aforementioned magnetic structures may readily be understood as the result of the co-operation and competition between the oscillatory indirect exchange, which is relatively strong in the heavy rare earths, because $(g-1)J$ is generally large, and the crystal-field and magnetoelastic anisotropy forces. The origin of the periodic structures can be explained by writing (1.4.21) in the form

$$\mathcal{H}_{\rm ff} = -\frac{N}{2}\sum_{\mathbf{q}} \mathcal{J}(\mathbf{q})\,\mathbf{J}(\mathbf{q})\cdot\mathbf{J}(-\mathbf{q}), \tag{1.5.4}$$

where the Fourier transform of the magnetic structure is

$$\mathbf{J}(\mathbf{q}) = \frac{1}{N}\sum_{i} \mathbf{J}_i e^{-i\mathbf{q}\cdot\mathbf{R}_i}. \tag{1.5.5}$$

In order to minimize the energy of the magnetic system, this term will favour a $\mathbf{Q}$ vector which corresponds to the maximum in $\mathcal{J}(\mathbf{q})$. The maxima shown in Fig. 1.17 thus reflect the observed $\mathbf{Q}$ values in the heavy rare earths through their position, and the relative stability of the periodic structures through their magnitude. The isotropic exchange does not in itself specify any orientation of the moments relative to the crystal axes. The normal to a planar helix can, for example, be rotated into an arbitrary direction without altering the exchange energy. This flexibility is realized in Eu, where the crystal-field anisotropy is very small because, like Gd, it has no ionic orbital moment. Neutron-diffraction studies of a single crystal by Millhouse and McEwen (1973) showed a first-order transition to a helical structure, and magnetization measurements indicate that the plane of the helical structure is always normal to the direction of a moderate applied field, even though $\mathbf{Q}$ remains along a four-fold axis of the bcc structure.

It is the magnetic anisotropy which fixes the magnetic structure relative to the crystal axes. As may be seen from eqn (1.4.4), the two-fold axial anisotropy (proportional to J_ζ^2) is also proportional to the Stevens factor α. If A_2^0 is negative throughout the heavy rare earths, as we shall see is the case, the values in Table 1.4 immediately explain why Tb and Dy have easy axes in the hexagonal plane, while the moments in Tm are strongly bound to the c-axis. In Ho and Er the higher-order axial anisotropy is important, but the values of α are consistent with the respectively large and small cone angles. Similarly, the alternation in the sign of γ in the series of the heavy elements is reflected in the easy directions of magnetization in the hexagonal plane. The competition between the exchange and the anisotropy is manifested in the low-temperature magnetic structures. In the ferromagnetic phases of Tb and Dy, the

anisotropy and magnetoelastic forces, which are averaged out or ineffective in the helical structure, are strong enough to overcome the relatively weak tendency to periodic ordering. In Tm, on the other hand, a compromise obtains, by which the moments take their maximum value along the c-axis, but alternate in direction so as to take advantage of the large peak in $\mathcal{J}(\mathbf{q})$. In Ho, the balance is so delicate that the weak classical dipolar interaction plays a crucial role, as we shall discuss in Section 2.3.

In order to explain the temperature dependence of the structures, it is necessary to determine the configuration of the moments which minimizes the *free energy*, taking into account the influence of increasing temperature and magnetic disorder on the interactions. Provided that the magnitude $|\langle \mathbf{J}_i \rangle|$ of the ordered moment is the same on all sites, the *entropy* term is independent of the details of the ordering (Elliott 1961), so the stable structure has the minimum *energy*. In exchange-dominated systems, like the heavy rare earths, the ordered moment approaches its saturation value at low temperature. As the temperature is increased, the structure which has the lowest energy may change as the effective interactions *renormalize*. This may occur either through a *second-order* transition, in which some *order-parameter* goes continuously to zero or, more commonly, discontinuously through a *first-order* transition. At elevated temperatures, the entropy may favour a structure, such as the longitudinal wave, in which the degree of order varies from site to site.

A conceptually simple but powerful means of calculating magnetic properties, and their dependence on the temperature, is provided by the molecular-field approximation or *mean-field theory*. We shall describe this method in some detail in the next chapter, but it is convenient to introduce it here in order to establish a few elementary results. The essential feature of the theory is the approximation of the two-ion interactions by effective single-ion terms, by replacing the instantaneous values of the $\mathbf{J}$ operators on the surroundings of any particular ion by their thermal averages. The effect of the exchange interaction (1.4.21) with the surrounding ions on the moment at $\mathbf{R}_i$ may then be written

$$\mathcal{H}_{\rm ff}(i) \simeq -(\mathbf{J}_i - \tfrac{1}{2}\langle \mathbf{J}_i \rangle) \cdot \sum_j \mathcal{J}(ij) \langle \mathbf{J}_j \rangle, \tag{1.5.6}$$

which in turn may be written in terms of an effective magnetic field

$$\mathbf{H}_{\rm eff}(i) = (g\mu_B)^{-1} \sum_j \mathcal{J}(ij) \langle \mathbf{J}_j \rangle, \tag{1.5.7}$$

plus a constant contribution to the energy. If the sum of the applied and effective fields is small, which will generally be true in the paramagnetic

phase (but not if spontaneous ordering occurs), the magnetic moment of the system per unit volume, neglecting the anisotropy, is given by Curie's law (1.2.32):

$$\mathbf{M} = \frac{g^2\mu_B^2 J(J+1)}{3k_B T}\frac{N}{V}(\mathbf{H}+\mathbf{H}_{\rm eff}). \tag{1.5.8}$$

For a uniform system, we may write

$$\mathbf{H}_{\rm eff} = \frac{1}{g^2\mu_B^2}\frac{V}{N}\sum_j \mathcal{J}(ij)\mathbf{M} = \frac{\mathcal{J}(\mathbf{0})}{g^2\mu_B^2}\frac{V}{N}\mathbf{M}, \tag{1.5.9}$$

recalling that

$$\mathcal{J}(\mathbf{q}) = \sum_j \mathcal{J}(ij)\, e^{-i\mathbf{q}\cdot(\mathbf{R}_i-\mathbf{R}_j)}, \tag{1.5.10}$$

and the susceptibility is therefore

$$\chi_{\rm MF} = \frac{g^2\mu_B^2 J(J+1)}{3k_B T}\frac{N}{V}\left[1-\frac{\mathcal{J}(\mathbf{0})J(J+1)}{3k_B T}\right]^{-1} \equiv \frac{C}{T-\theta}, \tag{1.5.11}$$

where C is the Curie constant (1.2.32), and the *paramagnetic Curie temperature* is

$$\theta = \frac{\mathcal{J}(\mathbf{0})J(J+1)}{3k_B}. \tag{1.5.12}$$

From the *Curie–Weiss law* (1.5.11) it is apparent that, if nothing else happens, the susceptibility diverges at θ, which is therefore also the Curie temperature T_C at which spontaneous ferromagnetism occurs in this model.

The bulk magnetic properties of the rare earths are summarized in Table 1.6, where the moments are given in units of μ_B/ion, and the temperatures in K. The theoretical paramagnetic moments per ion are $\mu = g\{J(J+1)\}^{1/2}\mu_B$, and are compared with values deduced from the linear magnetic susceptibilities in the paramagnetic phases, using (1.5.11). The theoretical saturation moments per ion are $g\mu_B J$, from (1.2.30), and are compared with low-temperature values, in fields high enough essentially to saturate the magnetization, or in the highest fields in which measurements have been made (McEwen *et al.* 1973). $\theta_{\parallel}$ and $\theta_{\perp}$ are the paramagnetic Curie temperatures, deduced from measurements with a field applied respectively parallel and perpendicular to the c-axis, and using (1.5.11). As we shall see in Section 2.1.1, there are corrections to this expression at finite temperatures, which give rise to a non-linearity in the inverse susceptibility. A simple linear extrapolation

therefore gives values for the paramagnetic Curie temperatures which depend on the highest temperature of the measurements. The fit to the experimental results for Tm illustrated in Fig. 2.1, for example, in which the mean-field corrections are taken into account, gives $\theta_{\parallel}$ and $\theta_{\perp}$ as respectively 52 K and -3 K, which differ significantly from the values deduced from a linear extrapolation of the same results, given in Table 1.6. A similar analysis for Er yields 69 K and 46 K. The ordering temperatures are determined either from bulk measurements or neutron diffraction. T_N and T_C denote transition temperatures to magnetically-ordered states without and with a net moment respectively, and values are given for sites of both kinds of symmetry, in the light rare earths.

Table 1.6. Magnetic properties of rare earth metals.

Metal	Para. moment		Sat. moment		$\theta_{\parallel}$	$\theta_{\perp}$	T_N		T_C
	μ	Obs.	gJ	Obs.			hex.	cub.	
Ce	2.54	2.51	2.14	0.6			13.7	12.5	
Pr	3.58	2.56	3.20	2.7[a]			0.05		
Nd	3.62	3.4	3.27	2.2[a]			19.9	8.2	
Pm	2.68		2.40						
Sm	0.85	1.74	0.71	0.13[a]			106	14.0	
Eu	7.94	8.48	7.0	5.1[a]				90.4	
Gd	7.94	7.98	7.0	7.63	317	317			293
Tb	9.72	9.77	9.0	9.34	195	239	230		220
Dy	10.65	10.83	10.0	10.33	121	169	179		89
Ho	10.61	11.2	10.0	10.34	73	88	132		20
Er	9.58	9.9	9.0	9.1	62	33	85		20
Tm	7.56	7.61	7.0	7.14	41	-17	58		32

[a] Values measured at 38 tesla.

A straightforward generalization of the above argument (see Section 2.1) gives the response of the ions in the paramagnetic phase to a spatially varying magnetic field with wave-vector $\mathbf{q}$. The corresponding susceptibility tensor (not to be confused with that for the conduction-electron gas) is

$$\chi_{\rm MF}(\mathbf{q}) = \frac{g^2\mu_B^2 J(J+1)}{3k_B T}\frac{N}{V}\left[1 - \frac{\mathcal{J}(\mathbf{q})J(J+1)}{3k_B T}\right]^{-1} = \frac{C}{T - T_N}. \tag{1.5.13}$$

Spontaneous ordering is therefore predicted to occur at the wave-vector

$\mathbf{Q}$ for which $\mathcal{J}(\mathbf{q})$ has its maximum value, and the Néel temperature is

$$T_N = \frac{\mathcal{J}(\mathbf{Q})J(J+1)}{3k_B}. \tag{1.5.14}$$

Since, from (1.4.22), $\mathcal{J}(\mathbf{q})$ varies as $(g-1)^2$, the critical temperature is expected to be proportional to the *de Gennes factor* $(g-1)^2J(J+1)$, provided that the susceptibility of the conduction-electron gas is constant. As may be seen from Tables 1.1 and 1.6, this relationship is rather accurately obeyed for the heavy rare earths, though not so well in the light elements. The crystal-field interactions influence the critical temperatures significantly, especially in the light end of the series, and both the electronic susceptibility and the matrix elements of the sf-exchange coupling, which together determine the indirect spin–spin interaction $\mathcal{J}_S(\mathbf{q})$, change through the series. The scaling of the critical temperature with the de Gennes factor is therefore more precise than would have been anticipated. The mean-field theory is known to be inadequate in the vicinity of the critical temperature, but as the rare earth metals are three-dimensional systems with long-range interactions, the transition temperature itself is rather well determined by this approximation. The theory is valid at high temperatures, and should describe the static magnetic structures adequately in the low-temperature limit. The discussion of the dynamical behaviour requires a time-dependent generalization of the mean-field, accomplished by the *random-phase approximation*. We shall later describe how low-temperature corrections to the mean-field properties may be derived from the magnetic-excitation spectrum, determined within the random-phase approximation. The discussion of the detailed behaviour close to the critical temperature, i.e. the *critical phenomena*, is however beyond the scope of this book, and we refer instead to the recent introduction to the subject by Collins (1989), and to the specialist literature on the application of statistical mechanics to phase transitions.

In mean-field theory, the exchange energy varies like σ^2, where the relative magnetization $\sigma(T)$ is $|\langle\mathbf{J}\rangle|/J$. However, the anisotropy energy generally changes more rapidly with magnetization. The crystal-field parameters B_l^m in (1.4.6) are generally assumed to vary only slightly with temperature, but the thermal average $\langle O_l^m(\mathbf{J})\rangle$ is very dependent on the degree of ordering. By treating the deviation in the direction of the moment on a particular site from the perfectly ordered state as a random walk on a sphere, Zener (1954) showed that

$$\left\langle O_l^m(\mathbf{J})\right\rangle_T = \left\langle O_l^m(\mathbf{J})\right\rangle_{T=0} \sigma^{l(l+1)/2}. \tag{1.5.15}$$

We shall discuss the derivation of this thermal average by mean-field theory in Section 2.2, and show that Zener's result is indeed correct at

low temperatures. Since the anisotropy energy is very small just below the critical temperature, the exchange dominates and gives rise to periodic magnetic structures in the heavy rare earths, except in Gd where the peak in $\mathcal{J}(\mathbf{q})$ occurs at $\mathbf{q} = \mathbf{0}$. As the temperature is lowered, the anisotropy forces become relatively more important, and phase transitions occur to structures in which their influence is apparent. A less obvious but nevertheless important effect is that $\mathcal{J}(\mathbf{q})$ itself changes substantially with temperature. As was mentioned in the last section, the peak reflects a maximum in the conduction-electron $\chi(\mathbf{q})$, which is determined by the form of the Fermi surface. Because of the interaction (1.3.23) between the local moments and the spins of the conduction electrons, the latter experience a potential with a period which is generally different from that of the lattice, and therefore generates extra energy gaps in the band structure. These *magnetic superzone* gaps, which we shall discuss in more detail in Section 5.7, may be of the order of 10 mRy and therefore perturb the energy spectrum of the conduction electrons significantly. In particular, the regions of the Fermi surface responsible for the peak in $\mathcal{J}(\mathbf{q})$ are severely modified, as has been verified through calculations on Tm by Watson *et al.* (1968). The result is that both the *position* of the peak is changed and its *magnitude* is reduced. As a consequence, periodic magnetic structures tend to be self-destructive; as they become established they try to eliminate the characteristic of the exchange which ensures their stability. These effects were studied by Elliott and Wedgwood (1964), who used a free-electron model to explain the variation of $\mathbf{Q}$ in the heavy metals. Although their model is greatly over-simplified, it illustrates the essential features of the problem. We shall see in Chapters 2 and 5 that this variation in $\mathcal{J}(\mathbf{q})$ is necessary to explain the change in both the magnetic structures and excitations with temperature.

Whereas the magnetic structures of the heavy rare earths can be accounted for by recognizing the dominant role of the exchange, and considering the crystal fields and magnetoelastic effects as perturbations, whose essential role is to establish favoured directions for the moments in the lattice, the balance in the light elements is not so clear-cut. Since g is generally close to 1, the exchange is relatively weak, and the larger values of $\langle r^l \rangle$ towards the beginning of the series are expected to make crystal-field effects relatively important. As a result, the latter are able to hinder the moments from attaining their saturation values of $g\mu_B J$, even in high fields at low temperatures, as illustrated in Table 1.6.

The most remarkable manifestation of the influence of the crystal fields is found in Pr, where they are able effectively to frustrate the efforts of the exchange to produce a magnetically ordered state. As illustrated in Fig. 1.16, the ground state on the hexagonal sites is the $|J_\zeta = 0>$

singlet which, in common with all singlet states, carries no moment. The first term in (1.2.24) therefore gives no contribution to the susceptibility, but the mixing of the $|\pm 1>$ excited doublet into the ground state by the field gives a Van Vleck susceptibility at low temperatures which, if we neglect the exchange, has the form

$$\chi = \frac{2g^2\mu_B^2 M_\alpha^2}{\Delta}\frac{N}{V}, \tag{1.5.16}$$

where $M_\alpha^2 = |<\pm 1|\, J_\alpha|0>|^2$ is the square of the matrix element of the component of $\mathbf{J}$ in the field direction, and Δ is the energy separation between the ground state and the first excited state. Since M_α is zero when the field is applied along the c-axis, no moment is initially generated on the hexagonal sites, as confirmed by the neutron diffraction measurements of Lebech and Rainford (1971), whereas the susceptibility in the basal plane is large. An applied field in the c-direction changes the relative energies of the crystal-field levels however, and at 4.2 K a field of 32 tesla induces a first-order *metamagnetic* transition to a phase with a large moment (McEwen *et al.* 1973), as shown in Fig. 7.13. This is believed to be due to the crossing of the ground state by the *second* excited state, as illustrated in Fig. 7.12.

If the exchange is included in the mean-field approximation, the $\mathbf{q}$-dependent susceptibility becomes, in analogy with (1.5.13),

$$\chi_{\rm MF}(\mathbf{q}) = g^2\mu_B^2\frac{N}{V}\left[\frac{\Delta}{2M_\alpha^2} - \mathcal{J}(\mathbf{q})\right]^{-1}. \tag{1.5.17}$$

From this expression, it is apparent that the susceptibility diverges, corresponding to spontaneous ordering, if

$$\frac{2\mathcal{J}(\mathbf{q})M_\alpha^2}{\Delta} \geq 1. \tag{1.5.18}$$

The magnetic behaviour of such a singlet ground-state system is therefore determined by the balance between the exchange and the crystal field. If the exchange is strong enough, magnetic ordering results; otherwise paramagnetism persists down to the absolute zero. In Pr, the crystal-field splitting is strong enough to preclude magnetic order, but the exchange is over 90% of that required for antiferromagnetism. We shall return to the consequences of this fine balance in Chapter 7.

The remaining close-packed light rare earths Ce, Nd, and Sm, which are amenable to experimental study (radioactive Pm is very intractable), all have an odd number of $4f$ electrons and thus, according to *Kramers' theorem*, crystal-field levels with even degeneracy and a magnetic moment. The crystal fields cannot therefore suppress magnetic ordering,

but they reduce the ordered moment and contribute to the complexity of the magnetic structures (Sinha 1978), which is exacerbated by the two different site-symmetries in each of the metals. The magnetic structure of Ce has not been fully determined, but it now seems (Gibbons *et al.* 1987) that commensurable transverse waves are formed on both the hexagonal and cubic sites, with **Q** in a b-direction and the moments pointing along an a-axis in the plane. The magnetic periodicity is twice that of the lattice. This relatively straightforward structure is in marked contrast to that of Nd, which displays an extraordinary complexity. An incommensurable longitudinal wave in a b-direction is formed on the hexagonal sites through a first-order transition at T_N, with a simple antiferromagnetic arrangement of successive hexagonal layers. As the temperature is lowered, a further first-order transition takes place within a degree to a double-**Q** structure (McEwen *et al.* 1985). At a still lower temperature, an incommensurable periodic structure in the b-direction is also formed on the cubic sites. At the lowest temperatures, the moments assume an elaborate quadruple-**Q** pattern (Forgan *et al.* 1989), which we shall discuss in more detail in Chapter 2. The magnetic structure on the hexagonal sites of Sm comprises pairs of planes with the moments arranged ferromagnetically in the c-direction (Koehler and Moon 1972). Adjacent pairs are coupled antiferromagnetically and separated by the cubic sites. The latter also order antiferromagnetically, with the moments along the c-axis, at low temperatures, but the normal to the ferromagnetic sheets is now in the b–c plane. Although the magnetic structures of the light rare earths are phenomenologically reasonably well described, the explanation of their origin in terms of the crystal-field and exchange interactions is still at a rudimentary stage.

The application of a magnetic field adds to the Hamiltonian a term

$$\mathcal{H}_Z = -g\mu_B \sum_i \mathbf{J}_i \cdot \mathbf{H}. \tag{1.5.19}$$

In a sufficiently large field, the stable configuration is thus an array of moments $g\mu_B J$ pointing along the field direction. The intermediate states between the zero-field structure and the high-field limit may however be very complex. In Fig. 1.20 on page 53 is shown a relatively simple example of the magnetization curves which result when a cone structure undergoes first-order transitions to the almost fully-aligned ferromagnetic state. We will discuss the effect of a magnetic field on periodic magnetic structures in some detail in Section 2.3, and therefore restrict ourselves for the moment to outlining the results of the mean-field treatment of Nagamiya *et al.* (1962) of the helical structure without planar anisotropy, to which a field is applied in the plane. The ferromagnetic

structure is reached at a field

$$H_c = \frac{J[\mathcal{J}(\mathbf{Q}) - \mathcal{J}(\mathbf{0})]}{g\mu_B}, \tag{1.5.20}$$

but there is an intermediate transition, occurring at approximately $H_c/2$, at which the helix transforms abruptly through a first-order transition to a *fan structure*, in which the moments make an angle θ with the field direction, given by

$$\sin\frac{\theta_i}{2} = \left\{\frac{2g\mu_B(H_c - H)}{J[3\mathcal{J}(\mathbf{Q}) - 2\mathcal{J}(\mathbf{0}) - \mathcal{J}(2\mathbf{Q})]}\right\}^{1/2} \sin \mathbf{Q}\cdot\mathbf{R}_i. \tag{1.5.21}$$

The opening angle of the fan thus goes continuously to zero at the second-order transition to the ferromagnetic phase.

The crystal fields manifest themselves in both microscopic and macroscopic magnetic properties. The macroscopic anisotropy parameters κ_l^m are defined as the coefficients in an expansion of the free energy in spherical harmonics, whose polar coordinates (θ, ϕ) specify the magnetization direction relative to the crystallographic axes. For hexagonal symmetry,

$$\begin{aligned} F(\theta,\phi) = N\big[&\kappa_0(T) + \kappa_2^0(T)P_2(\cos\theta) + \kappa_4^0(T)P_4(\cos\theta) \\ &+ \kappa_6^0(T)P_6(\cos\theta) + \kappa_6^6(T)\sin^6\theta\cos 6\phi\big], \end{aligned} \tag{1.5.22}$$

where $P_l(\cos\theta) = (4\pi/2l+1)^{1/2}Y_{l0}(\theta,\phi)$ are the Legendre polynomials. Anisotropic two-ion coupling and magnetoelastic strains may introduce additional higher-rank terms of the appropriate symmetry. If the Hamiltonian is written in a representation $\mathcal{H}(\theta,\phi)$ in which the quantization axis is along the magnetization, the macroscopic and microscopic parameters are related by

$$F(\theta,\phi) = -\frac{1}{\beta}\ln\,\mathrm{Tr}\big\{e^{-\beta\mathcal{H}(\theta,\phi)}\big\}. \tag{1.5.23}$$

Transforming the Stevens operators to a coordinate system with the z-axis along the magnetization direction, and assuming that the isotropic exchange is the dominant interaction, we find at absolute zero

$$\begin{aligned} \kappa_2^0(0) &= 2B_2^0J^{(2)} & \kappa_4^0(0) &= 8B_4^0J^{(4)} \\ \kappa_6^0(0) &= 16B_6^0J^{(6)} & \kappa_6^6(0) &= B_6^6J^{(6)} \end{aligned} \tag{1.5.24}$$

where

$$J^{(n)} \equiv J(J-\tfrac{1}{2})(J-1)\cdots(J-\tfrac{n-1}{2}). \tag{1.5.25}$$

There are a number of different experimental methods for obtaining values for the microscopic and macroscopic anisotropy parameters. The susceptibility in different directions, or equivalently the torque on a crystal in a field, can be measured either in the paramagnetic or magnetically ordered phases and, as we shall discuss in detail later, much information may be obtained from the excitation spectrum and its field dependence. The values of $\kappa_l^m(0)$ obtained from these various sources for the different elements have been reviewed and tabulated by McEwen (1978).

In order to deduce the crystal-field parameters B_l^m in the absence of exchange and magnetoelastic effects, Touborg and his collaborators studied the crystal-field states of dilute alloys of the magnetic rare earths in the non-magnetic hosts Sc, Y, and Lu, utilizing magnetization measurements and, to a limited extent, neutron spectroscopy. Their results for heavy rare earth solutes have been reviewed by Touborg (1977) and, for the light elements, by Touborg *et al.* (1978). Within the uncertainty of the measurements and of the interpretation, and with the exception of Ce in Y, which behaves anomalously, they found that a common set of parameters B_l^m/α_l accounts for the behaviour of all solutes in a particular host. B_4^0/β and B_6^0/γ are roughly 10 K/ion and 15 K/ion respectively in all cases, while B_6^6 is close to the value $-\frac{77}{8}B_6^0$ which the point-charge model would predict. B_2^0/α increases from about 30 K/ion in Sc, to 45 K/ion in Lu, to 100 K/ion in Y, which correlates with the deviation of the c/a ratio of the host metal (1.592 for Sc, 1.584 for Lu, and 1.573 for Y) from the ideal value of 1.633 (Orlov and Jensen 1988). It is noteworthy that the parameters B_l^m/α_l show no obvious correlation with $\langle r^l \rangle$, as would be anticipated from (1.4.4).

The values of B_l^m from these studies of dilute alloys may be compared with those from other sources. In particular, B_2^0 may be estimated for the pure metals by interpolating between the c/a ratios of the non-magnetic hosts. These values may then be compared with those deduced from the difference between the paramagnetic Curie temperatures parallel and perpendicular to the c-axis, which is shown in Section 2.1 to be given by

$$B_2^0 = \frac{5k_B(\theta_\perp - \theta_\parallel)}{6(J - \frac{1}{2})(J + \frac{3}{2})}. \tag{1.5.26}$$

The agreement for the heavy rare earths is in all cases good (McEwen 1978), indicating that the crystal fields measured in dilute alloys are related to those acting in the pure metals. On the other hand, the values deduced from torque and magnetization measurements at low temperatures in the ferromagnetic state show large discrepancies with those in the paramagnetic phase. For Tb and Dy, the former are roughly three times the latter. Despite this discrepancy, which is probably primarily

due to the anisotropic two-ion coupling in the magnetically ordered phases, the axial anisotropy parameter $\kappa_2^0(T)-\frac{5}{2}\kappa_4^0(T)+\frac{35}{8}\kappa_6^0(T)$, where $\kappa_2^0(T)$ is the dominating term, depends on temperature approximately as predicted by (1.5.15), varying roughly as σ^3 in Dy and σ^4 in Tb. We shall return to the question of the anisotropy parameters in the rare earths when we discuss the structures and excitations.

The large magnetoelastic effects have a profound effect on the magnetic properties of the rare earths, making a significant contribution to the anisotropy, playing a decisive role in some instances in determining the structures, and modifying the excitation spectrum. We here consider for illustrative purposes a special example, the basal-plane ferromagnet, exemplified by Tb and Dy. As mentioned previously, the α-strains maintain the symmetry and therefore only have the effect of renormalizing the B_l^m, and if the moments are confined to the plane, the ε-strains vanish. However, the γ-strains are large and symmetry-breaking, and thereby cause qualitative modifications in the magnetic behaviour. From (1.4.8) and (1.4.11), their contribution to the magnetoelastic Hamiltonian may be written

$$\begin{aligned}\mathcal{H}_\gamma = \sum_i \big[\tfrac{1}{2}c_\gamma(\epsilon_{\gamma 1}^2+\epsilon_{\gamma 2}^2) - B_{\gamma 2}\{O_2^2(\mathbf{J}_i)\epsilon_{\gamma 1}+O_2^{-2}(\mathbf{J}_i)\epsilon_{\gamma 2}\} \\ - B_{\gamma 4}\{O_4^4(\mathbf{J}_i)\epsilon_{\gamma 1}-O_4^{-4}(\mathbf{J}_i)\epsilon_{\gamma 2}\}\big],\end{aligned} \tag{1.5.27}$$

where we have included only the lowest ranks ($l=2$ and 4 respectively) of the $\gamma 2$ and $\gamma 4$ terms. As shown in Section 2.2, the condition

$$\partial F/\partial \epsilon_\gamma = 0 \tag{1.5.28}$$

leads to the equilibrium strains

$$\begin{aligned}\epsilon_{\gamma 1} &= \frac{1}{c_\gamma}\big(B_{\gamma 2}\langle O_2^2\rangle + B_{\gamma 4}\langle O_4^4\rangle\big) \\ \epsilon_{\gamma 2} &= \frac{1}{c_\gamma}\big(B_{\gamma 2}\langle O_2^{-2}\rangle - B_{\gamma 4}\langle O_4^{-4}\rangle\big).\end{aligned} \tag{1.5.29}$$

Transforming the Stevens operators as before, and using (1.5.15) to estimate the magnetization dependence of the thermal averages, we obtain

$$\begin{aligned}\epsilon_{\gamma 1} &= C\cos 2\phi - \tfrac{1}{2}A\cos 4\phi \\ \epsilon_{\gamma 2} &= C\sin 2\phi + \tfrac{1}{2}A\sin 4\phi,\end{aligned} \tag{1.5.30}$$

where

$$\begin{aligned}C &= \frac{1}{c_\gamma}B_{\gamma 2}J^{(2)}\sigma^3 \\ A &= -\frac{2}{c_\gamma}B_{\gamma 4}J^{(4)}\sigma^{10}\end{aligned} \tag{1.5.31}$$

are the conventional magnetostriction parameters (Mason 1954), and ϕ

is the angle between the a-axis and the magnetization in the plane.

The dominant contribution to the magnetoelastic energy is

$$\langle \mathcal{H}_\gamma \rangle = -\tfrac{1}{2} N c_\gamma (\epsilon_{\gamma 1}^2 + \epsilon_{\gamma 2}^2) = -\tfrac{1}{2} N c_\gamma (C^2 + \tfrac{1}{4} A^2 - CA \cos 6\phi). \quad (1.5.32)$$

The $\cos 6\phi$ term makes a contribution to the hexagonal anisotropy, which is in total, from (1.5.24), (1.5.15), and (1.5.31),

$$\begin{aligned} \kappa_6^6(T) &= B_6^6 J^{(6)} \sigma^{21} + \tfrac{1}{2} c_\gamma CA \\ &= B_6^6 J^{(6)} \sigma^{21} - \frac{1}{c_\gamma} B_{\gamma 2} J^{(2)} B_{\gamma 4} J^{(4)} \sigma^{13}. \end{aligned} \quad (1.5.33)$$

The hexagonal anisotropy can readily be deduced from the critical field H_c necessary to rotate the moments from an easy direction to a neighbouring hard direction in the plane (respectively a b-axis and an a-axis in Tb), which is given by

$$g\mu_B J \sigma H_c = 36 |\kappa_6^6(T)|. \quad (1.5.34)$$

Values of the critical field for Tb are given as a function of σ in Fig. 1.21.

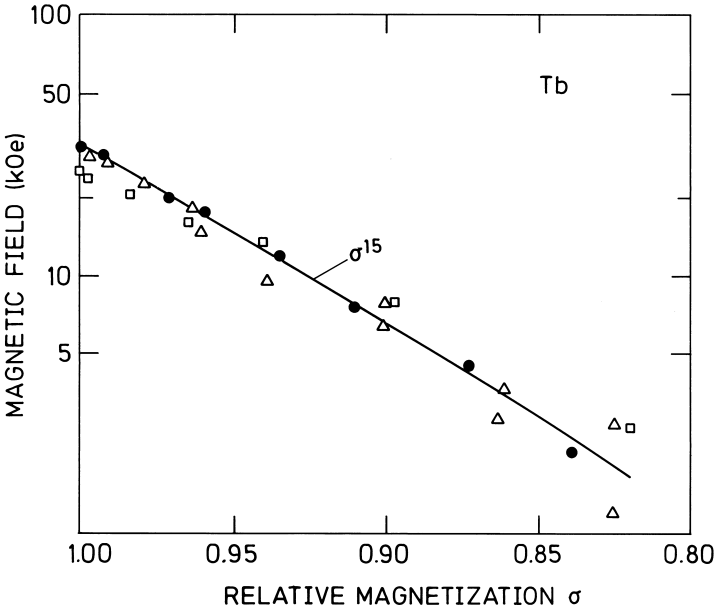

Fig. 1.21. The critical field H_c necessary to rotate the moments from an easy direction to a neighbouring hard direction in the plane in Tb, as a function of the reduced magnetization. The closed circles denote the results of neutron-scattering experiments, and the other signatures are deduced from macroscopic measurements.

The observed σ^{15} dependence on the magnetization indicates that the magnetoelastic term dominates. As illustrated in Fig. 1.22, C and A have been accurately determined by Rhyne and Legvold (1965a) from macroscopic strain-gauge measurements and, since the elastic constant is known (Jensen and Palmer 1979), the relative magnetoelastic and crystal-field contributions to (1.5.33) may readily be determined. At absolute zero, the former is 1.14 K/ion and the latter is −0.60 K/ion, rapidly becoming negligible as the temperature is increased. On account of the sign of the Stevens factor γ for Tb, the crystal-field contribution is expected to be positive, and this may be another indication of the importance of anisotropic two-ion coupling in the magnetically ordered phases.

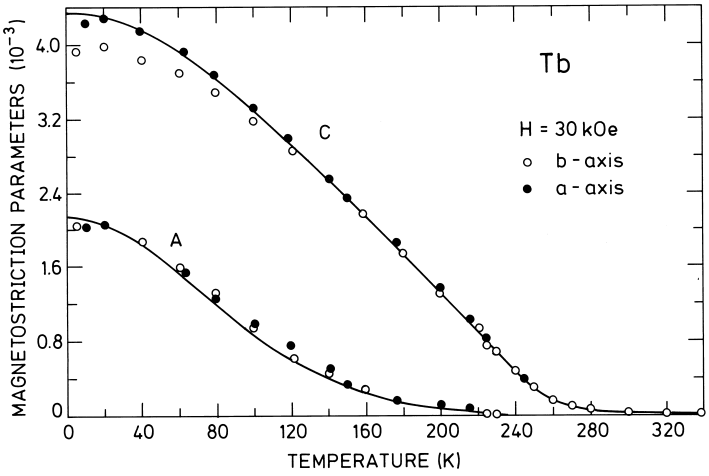

Fig. 1.22. The temperature dependence of the magnetostriction parameters C and A in Tb, after Rhyne and Legvold (1965a). The full lines show the results of the Callen-Callen theory presented in Section 2.2.

The magnetoelastic energy (1.5.32) is substantial in the ferromagnetic phase. In particular the term $-\frac{1}{2}c_\gamma C^2$, which results from a magnetoelastic strain of *cylindrical* symmetry, is relatively important at high temperatures, because it renormalizes roughly as σ^4, and is therefore still about 0.3 K/ion in Dy at 85 K, the temperature at which a first-order transition occurs from the helical to the ferromagnetic phase. The *hexagonally* symmetric contribution proportional to CA is small at all temperatures in Dy, since $A \approx 0$ (Martin and Rhyne 1977). In the helical phase, the lattice is *clamped* (Evenson and Liu 1969), so that the γ-strains are zero, and the magnetoelastic contribution to the stabilization energy is therefore absent. At T_C, this energy, plus a minor

contribution from the crystal-field anisotropy, just balances the difference in exchange energy between the helical and ferromagnetic phases:

$$\Delta U_{\rm ff} = -\tfrac{1}{2}NJ^2\sigma^2\{\mathcal{J}_h(\mathbf{Q}) - \mathcal{J}_f(\mathbf{0})\}. \qquad (1.5.35)$$

There has been some discussion about the relative importance of the two terms in stabilizing the ferromagnetic phase. From an analysis of the field required to induce the transition above T_C, Cooper (1968a) concluded that the magnetoelastic energy plays the dominant role. This conclusion was, however, based on the implicit assumption that the exchange energy changes little between the phases, and later measurements of the spin waves by Nicklow *et al.* (1971b) demonstrated that this is not the case. The energy difference $-\frac{1}{2}J^2\sigma^2\{\mathcal{J}_h(\mathbf{Q}) - \mathcal{J}_h(\mathbf{0})\}$ is about 2 K/ion in the helical phase, but the corresponding quantity is substantially smaller in the ferromagnetic phase. Del Moral and Lee (1975) reanalysed the data and concluded that the change (1.5.35) in the exchange energy makes the major contribution to driving the transition. Any statement about what drives a *first-order*, as distinct from a *second-order* transition must necessarily be imprecise, since all contributions to the energy change discontinuously at the transition. Immediately below T_N, the exchange dominates and the anisotropy forces are small. As the temperature is lowered, the peak in $\mathcal{J}(\mathbf{Q})$ decreases and moves, as was shown explicitly for the analogous case of Tb by the spin-wave measurements of Bjerrum Møller *et al.* (1967), illustrated in Fig. 6.1. The magnetoelastic forces therefore increase in relative importance, until a balance is reached and the transition to the ferromagnetic phase takes place. At the transition, a large change occurs in the exchange. Without the magnetoelastic term, T_C would be determined by the hexagonal crystal-field anisotropy, and would therefore be much lower. In this sense, the cylindrically-symmetric magnetoelastic forces drive the transition.